*International Journal of Physics and Mathematical Sciences ISSN: 2277-2111 (Online)*
*An Open Access, Online International Journal Available at http://www.cibtech.org/jpms.htm*
*2016 Vol. 6 (4) October-December, pp. 63-72/Sulochana*
***Research Article***

# SIMILARITY SOLUTION ON UNSTEADY AXI-SYMMETRIC VISCOUS BOUNDARY LAYER FLOW

***P. Sulochana**
*Department of Mathematics, Intell Engineering College, Ananthapuramu*
**Author for Correspondence*

**ABSTRACT**
In this paper, we have considered an incompressible viscous fluid in a three-dimensional axi-symmetric coordinate system. The governing equations are transformed to ordinary differential equations by using properly introduced similarity variable. Furthermore, pressure variations along the boundary layer thickness are taken into account. The energy equation is solved by Numerical technique. The fluid temperature, the velocity components and the solidification rate are presented for different values of non-dimensional governing parameters.

***Keywords:*** *Axisymmetric Solidification, Viscous Flow, Exact Solution, Stagnation Point, Unsteady Flow*

## INTRODUCTION

The manufacture of almost every man-made material involves the solidification process at some stage of the manufacturing process. Some of the important processes that involve solidification are foundry, welding, casting of ingots and continuous casting. Continuous casting is of such importance because it is a very economic method of forming a metallic component. The composition variation within a solidified product is known as segregation. Segregation in an alloy is a result of solute rejection at the solidification front followed by its redistribution by diffusion and mass flow. Depending on the extension of composition variation, this defect is classified as micro segregation, relative to grain scale, or macro segregation, relative to the product scale. Macro segregation affects the mechanical (ductility, strength, etc) and chemical properties (corrosion resistance) of materials in the product extension. It also affects precipitation of weak second phases, that was not expected if the initial composition was achieved, and porosity may be generated. Hence, Solidification is a two-phase phenomenon that is used in different natural processes and industrial applications. Glass, metal, plastic and oil industries, providing food and other corresponding industries needs a good insight of solidification behavior as the nature of solid growth. Studies of phase change in stagnant media for better understanding of convection effect upon the interface behavior and solidification properties are needed by industrial demand such as the desire for more homogenous semi-conductor crystals, in nuclear industry, as well as the better understanding of natural ice formation. The classic problem stagnant fluid solidifying on the cold plate is solved by Stefan (Stefan, 1891). One dimensional heat fluxes method for phase change problem is presented (Goodrich, 1978). These methods are accompanied simplified assumptions such as one dimensionality solid-liquid interface. An experimental study for natural convection in interface within heat flux controlling due to solidification is provided (Sparrow *et al.,* 1983). Also, a numerical method for solidifying in natural convection is used (Lacroix, 1989) and three dimensional problems for natural convection accompaniment phase change in rectangular channel is solved by Hadji and Schell (1990) in fluid variable properties state with temperature. Solidification of a fluid layer confined between two isolated plates is investigated by Hanumanth (1990). Another way for calculating of heat flux depended to on time in natural convection is presented by Oldenburg and Spera (1992). A combined model for phase change upon various states of pure substances, melting fluid problem due to spreading and solidifying on the flat plate and numerical modeling of forming and solidifying of a droplet on a cold plate is investigated by Trapaga *et al.,* (1992); Watanabe *et al.,* (1992); Marchi *et al.,* (1993). Evolution due to impact on substrate plate and solidifying of a droplet (Brattkus and Davis, 1988) is presented. But in concentrating upon stagnation flow, solidification of an inviscid fluid at interface and effect of its phenomena on morphological instability is investigated by Rangel and Bian (1994). Stefan problem for inviscid

stagnation flow by two methods and solidifying of super-cooled liquid stagnation inviscid flow is considered by Lambert and Rangel (2003); Yoo (2000), respectively. Recently, Shokrgozar and Rahimi (2012) studied the two-dimensional solidification of a viscous stagnation flow. In this paper, the exact solution of the momentum equations (Shokrgozar and Rahimi, 2013) is used for numerical solution of the energy equation. Imagine the fluid from far field moves perpendicularly approaches to a cold plate and after impinging on the plate the solid phase will formed on it gradually (Figure 1). In this study, the solidification process of a viscous stagnation flow is investigated in a three-dimensional axi-symmetric coordinate where a new method is implemented for validation of the numerical results. In this method, the exact solution of a heat profile is used as a quasi-steady solution for the problem. A parametric study is performed to examine influences of governing dimensionless parameters on the results as well. An exact solution is performed for solving momentum equations (Shokrgozar *et al.*, 2016) while the energy equation in liquid phase, solid-liquid interface and solid phase is solved by using finite difference method. The exact solution of the energy equation is used for validation of the numerical solution of energy equation, too. Forth order Runge-Kutta algorithm is used for solving momentum and energy equations. In addition, Numerical solution is needed to finding unsteady temperature profiles at each time step.

***Formulation and Solution of the Problem***

We consider unsteady viscous incompressible laminar stagnation flow with strain $a(t)$ perpendicularly approaches to a plate, along z-direction, initially positioned at $z=0$ when $t=0$. For all times of consideration, the fluid is solidified with variable solidification velocity and acceleration, $\dot{S}(t)$ and $\ddot{S}(t)$, respectively, that of an imaginary plate at solid-liquid interface is moved towards fluid where $S(t)$ is the plate distance, at time t, from the plate origin at $z=0$.

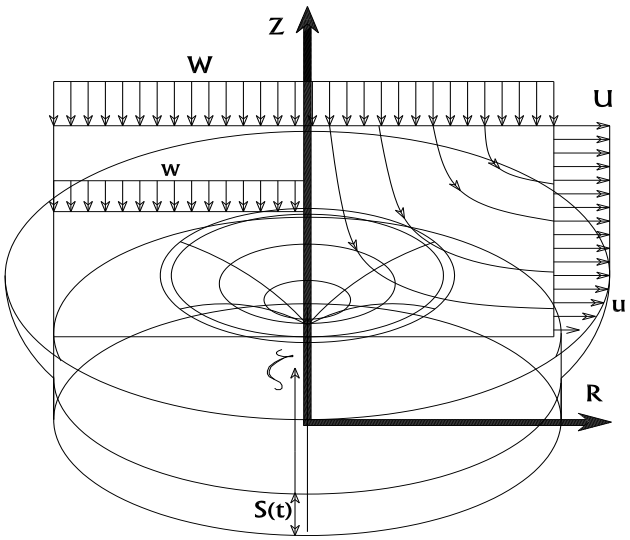


**Figure 1: Axi-symmetric Stagnation Flow (Coordinate System)**

Figure 1 represents three-dimensional axi-symmetric coordinates with corresponding $(u,w)$ velocities related to $(r,z)$. The imaginary plate is considered as a flat one because the only mechanism of heat transfer in the interface is conduction with the same temperature difference so the substrate remains flat. The inviscid flow can be assumed as potential flow within displacement thickness in boundary layer region. Where, $a_0$ is the strain rate at far field. For a Newtonian fluid with constant density and viscosity, unsteady three-dimensional axi-symmetric Navier-Stokes equations governing the flow and heat transfer are given as:

Mass, Momentum:

$$\frac{1}{r}\frac{\partial}{\partial r}(ru)+\frac{\partial w}{\partial z}=0 \quad (1)$$

$$\frac{\partial u}{\partial t}+u\frac{\partial u}{\partial r}+w\frac{\partial u}{\partial z}=-\frac{1}{\rho}\frac{\partial p}{\partial r}+\upsilon\left(\frac{\partial^2 u}{\partial r^2}+\frac{1}{r}\frac{\partial u}{\partial r}-\frac{u}{r^2}+\frac{\partial^2 u}{\partial z^2}\right) \quad (2)$$

$$\frac{\partial w}{\partial t}+u\frac{\partial w}{\partial r}+w\frac{\partial w}{\partial z}=-\frac{1}{\rho}\frac{\partial p}{\partial z}+\upsilon\left(\frac{\partial^2 w}{\partial r^2}+\frac{1}{r}\frac{\partial w}{\partial r}+\frac{\partial^2 w}{\partial z^2}\right) \quad (3)$$

In liquid phase: Energy (dissipation and radiation heat transfer are neglected without internal source):

$$\frac{\partial T}{\partial t}+u\frac{\partial T}{\partial r}+w\frac{\partial T}{\partial z}=\alpha\left[\frac{\partial^2 T}{\partial r^2}+\frac{1}{r}\frac{\partial T}{\partial r}+\frac{\partial^2 T}{\partial z^2}\right] \quad (4)$$

In solid phase

$$\frac{\partial T}{\partial t}=\alpha\left[\frac{\partial^2 T}{\partial r^2}+\frac{1}{r}\frac{\partial T}{\partial r}+\frac{\partial^2 T}{\partial z^2}\right] \quad (5)$$

At the interface

$$\rho h_{ls}\frac{dS(t)}{dt}=k_s\frac{\partial T_s}{\partial z}-k_l\frac{\partial T_l}{\partial z} \quad (6)$$

The conductivity and heat capacity coefficients are constant ($k$ and $c$ respectively) also $du\approx c\,dT$ is assumed where $p$, $\rho$, $\upsilon$, and $\alpha$ are the fluid pressure, density, kinematic viscosity, and thermal diffusivity, respectively. The dissipation terms are neglected in the energy equation because of the flow velocities being too small. Also, subscripts $s$ and $l$ denote solid and liquid, respectively.

According to Shokrgozar *et al.*, (2016), viscous parts of the velocity components are as:

$$u=a(t)\,r\,f'(\eta) \quad (7)$$

$$w=-2\sqrt{\upsilon/a_\circ}\;a(t)\,f(\eta) \quad (8)$$

$$\eta=\sqrt{\upsilon/a_\circ}\,\zeta \quad \text{,and} \quad \zeta=z-S(t) \quad (9)$$

In which the terms involving $f(\eta)$ in (7), (8) comprise the axi-symmetric similarity form for unsteady stagnation flow, and prime denotes differentiation with respect to $\eta$. Transformations (7)-(9) satisfy (1) automatically and their insertion into (2)-(3) yields an ordinary differential equation in terms of $f(\eta)$ along with an expression for the pressure, as follow:

$$f'''+f''\left(\tilde{\dot{S}}+2\tilde{a}f\right)+\left(-\tilde{a}\,f'-\frac{1}{\tilde{a}}\frac{d\tilde{a}}{d\tau}\right)f'-\frac{1}{\tilde{a}\,\xi}\frac{\partial\tilde{P}}{\partial\xi}=0 \quad (10)$$

$$\tilde{p}-\tilde{p}_\circ=-2\tilde{a}\left(\tilde{a}f^2+f'+\tilde{\dot{S}}f\right)-\frac{\xi^2}{2}\left(\frac{\partial\tilde{a}}{\partial\tau}+\tilde{a}^2\right)+\int_0^\eta 2\frac{\partial\tilde{a}}{\partial\tau}f\,d\eta \quad (11)$$

In which,

$$-\frac{1}{\tilde{a}\,\xi}\frac{\partial\tilde{P}}{\partial\xi}=\frac{1}{\tilde{a}}\frac{\partial\tilde{a}}{\partial\tau}+\tilde{a} \quad (12)$$

$$\frac{\partial\tilde{a}}{\partial\tau}=\frac{\tilde{\dot{S}}}{\eta_\circ}+\frac{\tilde{\dot{S}}^2}{\eta_\circ^2}+\frac{\tilde{W}_\circ\tilde{\dot{S}}}{\eta_\circ^2} \quad (13)$$

$$\tilde{P}(r,z,t)=\frac{p(r,z,t)}{\rho a_{\circ}\upsilon}\ ,\ \tilde{S}(t)=\sqrt{a_{\circ}/\upsilon}\,S(t)\,,\ \tilde{a}(t)=\frac{a(t)}{a_{\circ}}\ ,$$
$$\dot{\tilde{S}}(t)=\dot{S}(t)\Big/\sqrt{a_{\circ}\ \upsilon}\ \ ,\ \xi=\sqrt{a_{\circ}/\upsilon}\ \ r \qquad (14)$$

Where dot denotes differentiation with respect to $t$, Also, $\tilde{P},\tilde{S},\dot{\tilde{S}}$ and $\tilde{r}$ are dimensionless forms of $P,S,\dot{S}$ and $r$, respectively.

The boundary conditions for the differential equation (10) are:

$$\eta=0:\quad f=0,\quad f'=0 \qquad (15)$$

$$\eta\to\infty:\quad f'=1 \qquad (16)$$

It is worth mentioning that relation (11) which represents pressure is obtained by integrating Equation (3) in z-direction and by use of the potential flow solution as boundary conditions.

To transform the energy equation into a non-dimensional form for the case of defined wall temperature, we introduce:

$$\theta=\frac{T(\eta)-T_{\infty}}{T_w-T_{\infty}} \qquad (17)$$

Making use of transformations (7) - (9), this equation may be written as:

$$\theta''+\left(\dot{\tilde{S}}(\tau)+2\ f\right)\ Pr.\theta'\ =0 \qquad (18)$$

With boundary conditions as:

$$\theta=1\ \text{ at }\ \eta=0 \qquad (19)$$

$$\theta=0,\quad \text{at}\quad \eta\to\infty \qquad (20)$$

Where, $\theta$ is dimensionless temperature, the subscript $w$ and $\infty$ refer to the conditions at the wall and in the free stream, respectively, and prime indicates differentiation with respect to $\eta$.

Using the non-dimensional quantities for temperature as $\theta$, time as $\tau$, distance from $r$ axis as $\tilde{r}$, and distance from $z$ axis as $\tilde{z}$, equations (4)-(6) become:

For liquid phase:

$$\frac{\partial\theta_l}{\partial\tau}+\tilde{u}\frac{\partial\theta_l}{\partial\tilde{r}}+\tilde{w}\frac{\partial\theta_l}{\partial\tilde{z}}=\alpha_l\left(\frac{\partial^2\theta_l}{\partial\tilde{r}^2}+\frac{1}{\tilde{r}}\frac{\partial\theta_l}{\partial\tilde{r}}+\frac{\partial^2\theta_l}{\partial\tilde{z}^2}\right) \qquad (21)$$

For solid phase:

$$\frac{\partial\theta_s}{\partial\tau}=\alpha_s\left(\frac{\partial^2\theta_s}{\partial\tilde{r}^2}+\frac{1}{\tilde{r}}\frac{\partial\theta_s}{\partial\tilde{r}}+\frac{\partial^2\theta_s}{\partial\tilde{z}^2}\right) \qquad (22)$$

And for their intersection:

$$\frac{Pr}{St}\frac{d\tilde{S}}{d\tau}=\frac{1}{k_r}\frac{\partial\theta_s}{\partial\tilde{z}}-\frac{\partial\theta_l}{\partial\tilde{z}} \qquad (23)$$

At first, the momentum equation of liquid (10) is solved numerically using a shooting method based on Runge-Kutta algorithm. Resulted velocities are used in energy equation (21) in liquid region in order to convert this nonlinear equation to a linear one. Then, this linear equation is dischretized by using Power Law scheme so for small $Pe(Pe<1)$ and Large $Pe(Pe>10)$, scheme is central and upwind, respectively. For $1<Pe<10$, scheme is composite of these two. For solving the algebraic system of equations, TDMA[i] within ADI[ii] method is used. In addition, the resulted velocities of momentum solution are used to obtain the exact solution of energy equation (Shokrgozar *et al.,* 2016). However, this exact solution is not used to capture the fluid temperature in the computational domain at each time step. In the next sections, the reason of this phenomenon will be discussed.

## RESULTS AND DISCUSSION

In this section, in order to validate the energy equation numerical results of our study, the obtained results are compared with exact solution and previous studies. Comparison of results between this study and exact solution is new and creative method. For comparisons, Shokrgozar *et al.,* (2013) study results are the most complete study and best selection. This reference was selected to validate the achieved results. For simplification and more excellent comparisons, parameter introducing in this study is the same as (Shokrgozar *et al.*, 2013) study. The results of these two studies are presented together in figure 3 for $\left(Pr=1,\ St=1,\ \theta_i=1,\ \alpha_r=1,\ k_r=1\right)$.

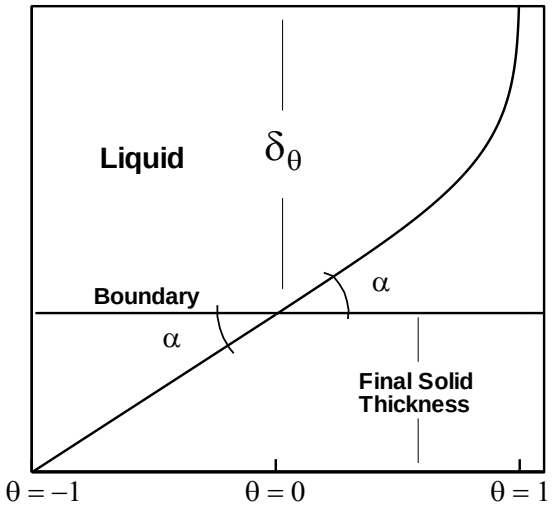


**Figure 2a: Final Solid Thickness, Low *Pr* Number**

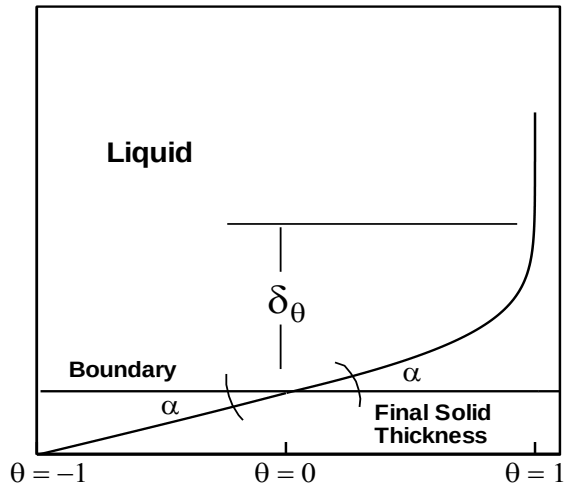


**Figure 2b: Final Solid Thickness, High *Pr* Number**

According to this figure, there is a difference in ultimate solid thickness between two-dimensional and three-dimensional cases, as expected; however, the trend of evolution is the same in both graphs. In addition, the exact solution of energy equation can be used for validation of the numerical solution of the same equation.

Figure 8 shows the comparison between exact and numerical solutions of temperatures profiles. Indeed, the exact solution is a quasi steady solution of the energy equation. This means the numerical solution is the same as the exact solution if there is enough time for evolution while other conditions are maintained constant.

In this figure, two profiles are matched completely, at first and last times. At the beginning, the time of evolutions is very small and differences between these two profiles are negligible (two profiles are matched completely). At the end, there is enough time to complete the evolution of temperature profile while variations of other parameters are not considerable as they are very close to reach their steady conditions.

In the middle times, there is a noticeable difference between two profiles expectedly; however, the trend of the profiles evolution at both figures is the same.

Figure 4 represents the temperature profiles of liquid and solid phases for different times due to advancement of solidifying front. The slope of each chart is $tg(\alpha)$ in the first node of liquid or solid phase. The figure reveals that solidification is stopped just as values of these two slopes become equal (note that $\alpha_r=1$).

Figure 5 presents the exact solution of thermal profile for different times and different solidification front velocity. Next, Figures 6 and 7 provide the velocity profiles in $r$ and $z$ directions for different times and

solid thicknesses. As it is shown, when the solidification velocity is very high, that is just for initial moments, the slope of velocity profile in boundary layer is very steep and the velocity approaches toward potential flow very fast and so the thickness of viscous boundary layer is very thin. By decreasing solidification velocity, Hiemenz flow is appeared more and more.
Also, a comparison is made in Figure 8 between exact and numerical solutions of heat transfer profiles at different times.

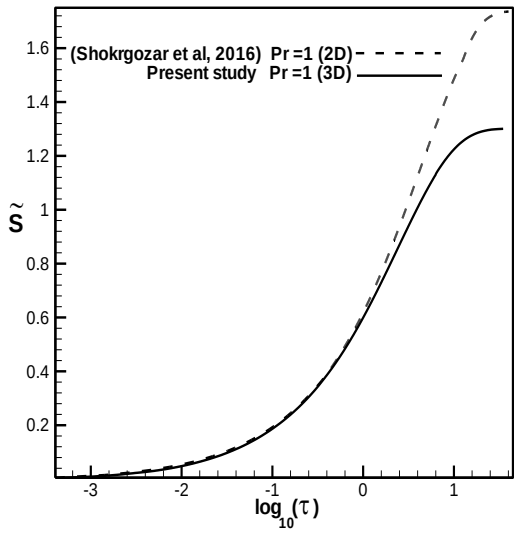


**Figure 3: Comparison of Two-Dimensional (Shokrgozar *et al.*, 2016) and Three-Dimensional (Present Study) Results for** $Pr=1, St=1, K_r=1, \alpha_r=1, \theta_I=1$

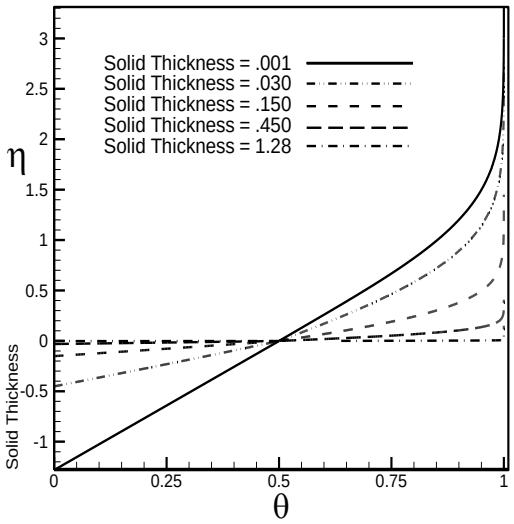


**Figure 4: Numerical Solution, Thermal Liquid and Solid Profiles for** $Pr=1, St=1, K_r=1, \alpha_r=1, \theta_I=1$

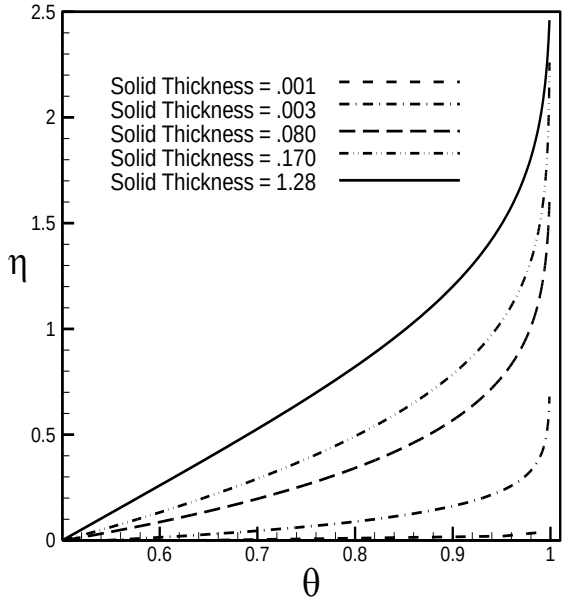


**Figure 5: Exact Solution, Thermal Profile for** $Pr=1, St=1, K_r=1, \alpha_r=1, \theta_I=1$

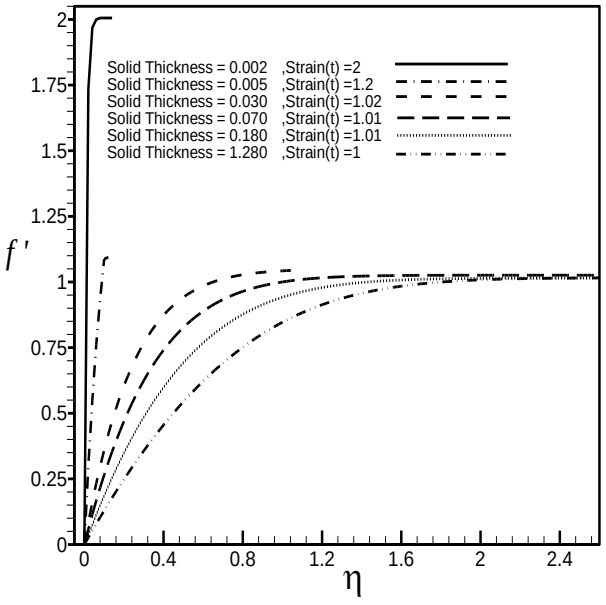


**Figure 6: Velocity Profile in** $x$ **Direction for** $Pr=1, St=1, K_r=1, \alpha_r=1, \theta_I=1$

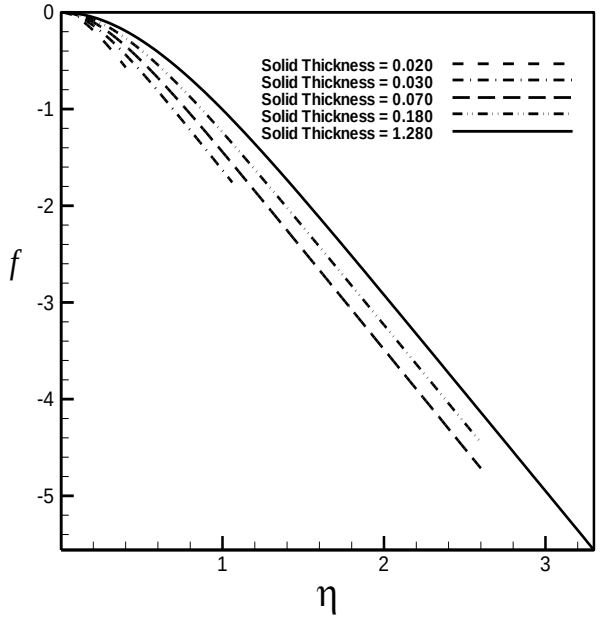


**Figure 7: Velocity Profile in $z$ Direction for $Pr=1, St=1, K_r=1, \alpha_r=1, \theta_I=1$**

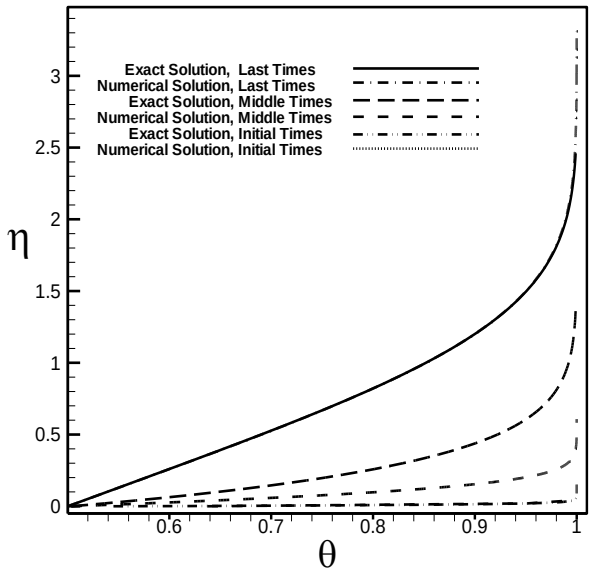


**Figure 8: Comparison between Temperatures Profile of Exact Solution and Numerical Solution $Pr=1, St=1, K_r=1, \alpha_r=1, \theta_I=1$**

The parametric studies are applied for different values of $Pr, St, \theta_I, K_r, \alpha_r$ while study is concentrated on the advancement of solidifying front versus time that is the most important phenomenon in solidification. In Figure 9, a comparison is made between the solidification process of this study and Ref. (Shokrgozar *et al.*, 2013) for $Pr=1$, $Pr=10$ and $Pr=0.1$, respectively.

The trend is the same in the two graphs so the solid upper limit decreases as $Pr$ number increases relatively to basic $Pr=1$ graph. Mathematical analysis can confirm the validity of the numerical solution. Solidification will stop when the steady conduction heat transfer establishes in intersection. One-dimensional steady conduction heat transfer at intersection reads:

$$\Delta\tau = \frac{Pr.\Delta\tilde{z}^2}{St}\frac{1}{\theta_{liquid}+\theta_{solid}/\alpha_r}$$

that the just upper and lower nodes temperature in fluid and solid regions are introduced by $\theta_{liquid}$ and $\theta_{solid}$, respectively. In this equation, dimensionless time ($\Delta\tau$) tends to infinity as $(\theta_{liquid}+\theta_{solid}/\alpha_r)\to 0$ and solidification is stopped consequently while $\alpha_r=1$ is assumed for simplification. It can be referred to (Shokrgozar *et al.*, 2013) for more details.

Figures 2A and 2B determine the ultimate solid thickness that is equal to $tg(\alpha)$ (where $tg(\alpha)$ is slope of temperature profile at first node). It is evident that when the thickness of the temperature boundary layer increases, the solid upper limit increases and this increasing is due to $Pr$ number decrease and vice versa. Moreover, it was capture that by taking into account solely the effect of $St$ number does not change the solid upper limit as $St$ number does not appear in (24) but $St$ number variations changes the solidification time.

However, a complete match of the heat transfer profiles obtained by two methods of exact solution and numerical solution at the beginning and ending times can be considered as the best reason for validation of the numerical results.

*International Journal of Physics and Mathematical Sciences ISSN: 2277-2111 (Online)*
*An Open Access, Online International Journal Available at http://www.cibtech.org/jpms.htm*
*2016 Vol. 6 (4) October-December, pp. 63-72/Sulochana*
***Research Article***

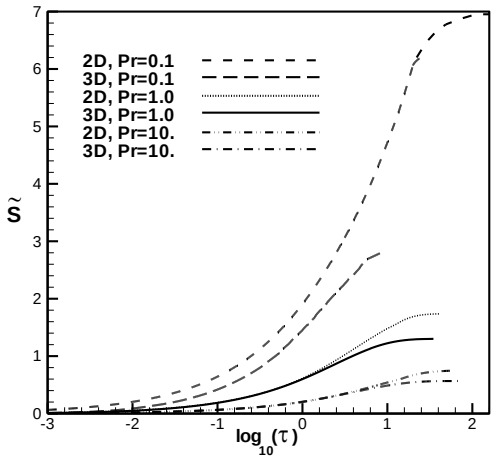


**Figure 9: Comparison between Two-Dimensional and Three-Dimensional; Effect of $Pr$ Number upon Solidification Front for $St=1,K_r=1,\alpha_r=1,\theta_I=1$**

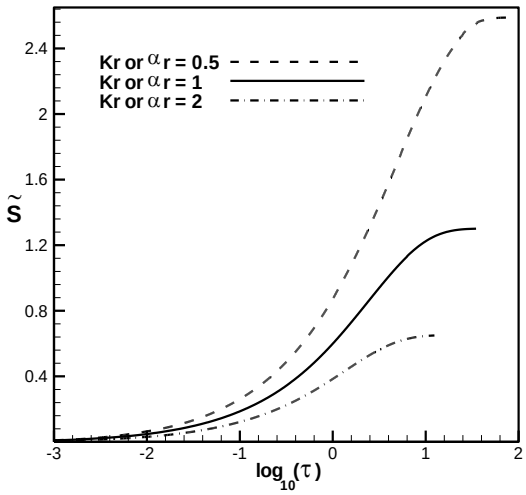


**Figure 10: Effect of $k_r$ or $\alpha_r$ Variations upon Solidification Front for $Pr=1,St=1,\theta_I=1$**

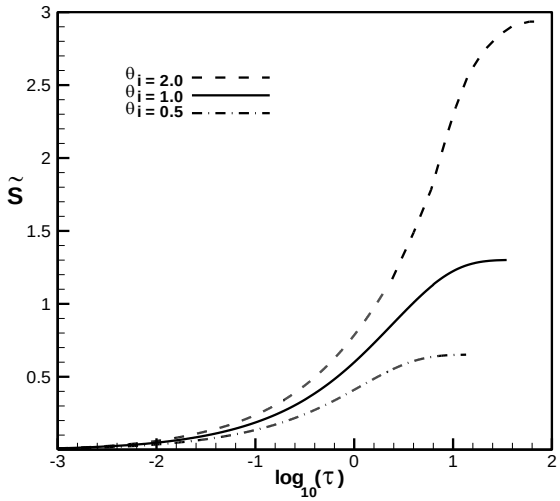


**Figure 11: Effect of $\theta_I$ Variations upon Solidification Front for $Pr=1,St=1,K_r=1,\alpha_r=1$**

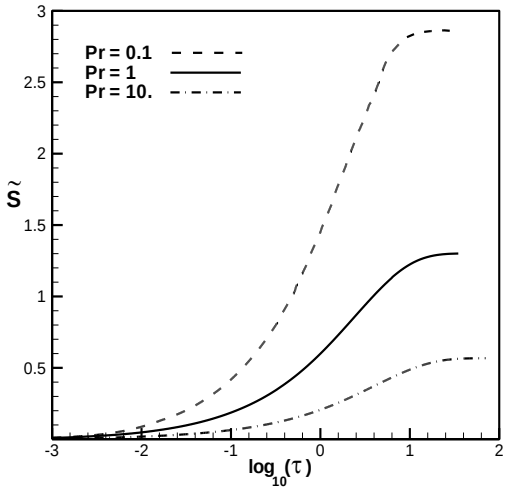


**Figure 12: Effect of $Pr$ Number upon Solidification Front for $St=1,K_r=1,\alpha_r=1,\theta_I=1$**

Equation (24) shows that decreasing of $k_r$ or $\alpha_r$ by half, increases solid upper limit two times exactly of that $tg(\alpha)$ increases two times (figure 2). Also, Figure 10 shows the effect of $k_r$ and $\alpha_r$ variations upon solidification front thickness. In this case, decreasing of $k_r$ and $\alpha_r$ by half, increases thickness of solid two times exactly. Figure 11 represents results for $\theta_I=0.5$ and $\theta_I=2$ ($Pr=1,St=1,k_r=1,\alpha_r=1$). The variations of $\theta_I$ have interesting results. When $\theta_I$ tends to zero, ultimate frozen thickness tends to infinity and this case requires another study separately. Figure 12 represents effect of $Pr$ number variations in front solidification more clearly. As previously mentioned, this figure shows increasing $Pr$ number decreases solid upper limit and vice versa. Figure 13 represents $St$ number has no effect on the ultimate thickness in front solidification as former discussion. However, the $St$ number has only effect upon the solidifying time.

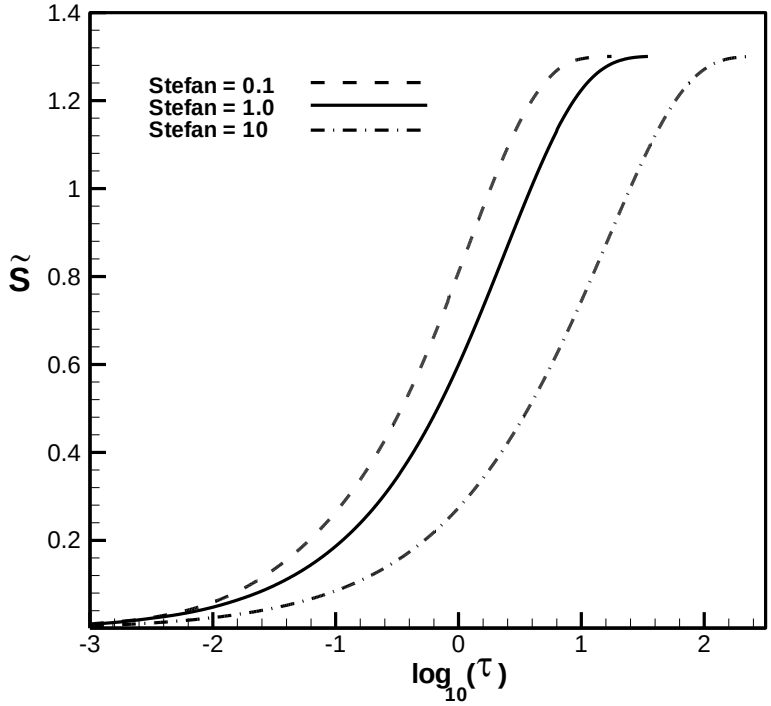


**Figure 13: Effect of** $St$ **Number upon Solidification Front for** $Pr=1, St=1, K_r=1, \alpha_r=1$

***Conclusion***

We have considered an incompressible viscous fluid in a three-dimensional axi-symmetric coordinate system. The governing equations are transformed to ordinary differential equations by using properly introduced similarity variable. The conclusions are made as the following.

1. The results show steady temperature boundary layer or, by more exact words, start of steady temperature profile slope determines the ultimate solidification thickness.
2. The ratio of liquid to solid temperature diffusivity and, more importantly, Pr number has effect upon this temperature boundary layer thickness.
3. Very small effect of convection terms at near of interface leads to flatting solidification front but these terms are very important as approaching to the edge of boundary layer.
4. The final solid thickness in a three-dimensional stagnation flow is about $0.75$ times of that of a two-dimensional case.

**REFERENCES**

**Brattkus K and Davis SH (1988).** Flow induced morphological instabilities: stagnation-point flows. *Journal of Crystal Growth* **89** 423-427.

**Goodrich LE (1978).** Efficient numerical technique for one dimensional thermal problems with phase change. *International Journal of Heat Mass Transfer* **21** 615-621.

**Hadji L and Schell M (1990).** Interfacial pattern formation in the presence of solidification and thermal convection. *Physical Review A* **41** 863-873.

**Hanumanth GS (1990).** Solidification in the presence of natural convection. *International Communications in Heat and Mass Transfer* **17** 283-292.

**Lacroix M (1989).** Computation of heat transfer during melting of a pure substance from an isothermal wall. *Numer. Heat Transfer B* **15** 191-210.

**Lambert RH and Rangel RH (2003).** Solidification of a super cooled liquid in stagnation-point flow. *International Journal of Heat Mass Transfer* **46** 4013-4021.

**Marchi CS, Liu H, Lavernia EJ and Rangel RH (1993).** Numerical analysis of the deformation and solidification of a sigle droplet impinging on to a flat substrate. *Journal of Materials Science* **28** 3313-3321.

**Oldenburg CM and Spera FJ (1992).** Hybrid model for solidification and convection. *Numerical Heat Transfer B* **21** 217-229.

**Rangel RH and Bian X (1994).** The inviscid stagnation-flow solidification problem. *International Journal of Heat Mass Transfer* **39**(8) 1591-1602.

**Shokrgozar A and Rahimi AB (2012).** Investigation of Two-dimensional unsteady stagnation point-flow and heat transfer impinging on an accelerated flat plate. *Journal of Heat Transfe*r **134** 064501-5.

**Shokrgozar A and Rahimi AB (2013).** Solidification of Two-Dimensional viscous, incompressible Stagnation flow. *International Journal of Heat Transfer* **135** 072301-8.

**Shokrgozar A, Rahimi AB and Mozayyeni H (2016).** Investigation of three-dimensional axisymmetric unsteady stagnation point-flow and heat transfer impinging on an accelerated flat plate. *Journal of Applied Fluid Mechanics* **9** 451-461.

**Sparrow EM, Ramsey JW and Harris S (1983).** The transition from natural convection controlled freezing to conduction controlled freezing. *Journal of Heat Transfer* **103** 7-13.

**Stefan J (1891).** Uber die theorie der eisbildung, insbesondere uber die eisbildung in polarmaere. *Annalen der Physik und Chemie* **42** 269-286.

**Trapaga G, Matthys EF, Valecia JJ and Szekely J (1992).** Fluid Flow, heat transfer and solidification of molten metal droplets impinging on substrates: comparison of numerical and experimental results. *Metallurgical Transactions B* **23B** 701-718.

**Watanabe T, Kuribayashi I, Honda T and Kanzawa A (1992).** Deformation and solidification of a droplet on a cold substrate. *Chemical Engineering Science* **47**(12) 3059-3065.

**Yoo JS (2000).** Effect of viscous plane stagnation flow on the freezing of fluid. *International Journal of Heat and Fluid Flow* **21** 735-739.